Juxtaposed membranes underpin cellular adhesion and display unilateral cell division of multicellular magnetotactic prokaryotes

Xin-xin Qian, Claire-lise Santini, Artemis Kosta, Nicolas Menguy, Hugo Le Guenno, Wenyan Zhang, Jinhua Li, Yi-ran Chen, Jia Liu, Francois Alberto, et al.

Juxtaposed membranes underpin cellular adhesion and display unilateral cell division of multicellular magnetotactic prokaryotes

Xin-Xin Qian [a, b], Claire-Lise Santini [a, b], Artemis Kosta [c], Nicolas Menguy [b, d], Hugo Le Guenno [c], Wenyan Zhang [b, e], Jinhua Li [b, f], Yi-Ran Chen [b, e,1], Jia Liu [b, e,2], François Alberto [a, b], Leon Espinosa [a], Tian Xiao [b, e], Long-Fei Wu [a, b,3]

a Aix Marseille University, CNRS, LCB, Marseille, 13402, France

b International Associated Laboratory of Evolution and Development of Magnetotactic Multicellular Organisms (LIA-MagMC), CNRS-CAS, Marseille, 13402, France

c Microscopy Core Facility, FR3479 IMM, CNRS, Aix Marseille University, Marseille, France

d Sorbonne Université, UMR CNRS 7590, Muséum National d'Histoire Naturelle, IRD, Institut de Minéralogie, de Physique des Matériaux et de Cosmochimie, IMPMC, 75005 Paris, France

e CAS Key Laboratory of Marine Ecology and Environmental Sciences, Institute of Oceanology, Chinese Academy of Sciences, Qingdao, 266071, China

f Key Laboratory of Earth and Planetary Physics, Institute of Geology and Geophysics, Chinese Academy of Sciences, Beijing, 100029, China

1 current address: LAAS, CNRS, 7 avenue Colonel Roche, 31400 Toulouse cedex 4, France

2 current address: Key Laboratory of Earth and Planetary Physics, Institute of Geology and Geophysics, Chinese Academy of Sciences, Beijing, 100029, China

3 To whom correspondence should be addressed: Long-Fei WU, LCB, CNRS, 31 chemin Joseph Aiguier, 13402 Marseille cedex 20, France, 33-4-91164157, wu@imm.cnrs.fr

Running head: Diversity and architecture of MMPs

Summary

Multicellular magnetotactic prokaryotes (MMPs) exhibit peculiar coordination of swimming along geomagnetic field lines. Approximate 40-80 cells assemble, with a helical geometry or axisymmetry, into spherical or ellipsoidal MMPs, respectively. To contribute to a comprehensive understanding of bacterial multicellularity here we took multiple microscopic approaches to study the diversity, assembly, reproduction and motility of ellipsoidal MMPs. Using correlative fluorescence *in situ* hybridization and scanning electron microscopy analysis, we found an unexpected diversity in populations of ellipsoidal MMPs in the Mediterranean Sea. The high-pressure freezing/freeze substitution fixation technique allowed us to show, for the first time, that cells adhere via juxtaposed membranes and are held together by a rimming lattice. Fluorescence confocal microscopy and ultra-thin section images revealed not only the one-layer hollow three-dimensional architecture, but also periphery–core unilateral constriction of constituent cells and unidirectional binary fission of the ellipsoidal MMPs. This finding suggests the evolution toward MMPs multicellularity via the mechanism of incomplete separation of offspring. Remarkably, thousands of flagellar at the periphery surface of cells underpin the coordinated swimming of MMPs in response to mechanical, chemical, magnetic and optical stimuli, including a magnetotactic photokinesis behavior. Together these results unveil the unique structure and function property of ellipsoidal MMPs.

Originality-Significance Statement

The hollow polar organization, unidirectional division of reproduction and mechano-magneto-photosensitive and coordinated swimming, justify multicellular magnetotactic prokaryotes as an attractive model organism in the study of evolution of multicellularity and mechanism of magnetoreception.

Introduction

Multicellularity evolved independently and repeatedly through two major mechanisms, incomplete separation of daughter cells after division and motile cell aggregation (Bonner, 1999). Morphological development results in the unbranched filaments with differentiated cells of cyanobacteria, the branched syncytial filaments of actinomycetes, and the fruiting bodies of myxobacteria (Claessen et al., 2014). These multicellular bacteria reproduce, besides binary cell fission, by sporulation or fragmentation of filaments to form propagules. The major modes of multicellular motility appear as the motile filaments of cyanobacteria and the social foraging for food by swarming myxobacteria (Claessen et al., 2014). Other types of multicellular prokaryotes with distinct features of multicellularity remain poorly investigated.

During the evolution various organisms have developed magnetoreception capacity to exploit geomagnetic field as an orientation cue and maps while migrating or homing (Johnsen and Lohmann, 2005). Several hypotheses have been proposed to account for the mechanism of

64 the magnetoreception. Increasing evidence supports a potential compass function of
65 magnetite particles in magnetotactic bacteria (MTB). MTB consist of a heterogeneous group
66 of Gram-negative bacteria that are capable of producing single domain magnetite (Fe_3O_4) or
67 greigite (Fe_3S_4) crystals in intracellular organelles termed magnetosomes (Bazylinski and
68 Frankel, 2004). The magnetosomes enable bacteria to align to and swim along geomagnetic
69 field lines, a behavior is referred to as magnetotaxis. The hypothetic function of magnetotaxis
70 is to simplify a three-dimensional search to a one-dimensional movement for cells to
71 efficiently find and maintain at the preferable oxic-anoxic transition zone in chemically
72 stratified sediments (Bazylinski and Frankel, 2004). Besides the most abundant unicellular
73 MTB, a group of multicellular magnetotactic prokaryotes (MMPs) has attracted particularly
74 our interest because they have opted both multicellular and magnetotactic properties during
75 their evolution.
76 Multicellular magnetotactic prokaryotes were first discovered in the Rodrigo de Freitas
77 lagoon in Brazil by Farina et al. (Farina et al., 1983). Typically, 15–45 bacterial cells arrange
78 with a helical geometry in a spherical or mulberry-like multicellular entity (Keim et al., 2006).
79 This type of MMPs has been observed worldwide (Rodgers et al., 1990; Simmons and
80 Edwards, 2007; Winklhofer et al., 2007; Wenter et al., 2009; Shapiro et al., 2011; Zhou et al.,
81 2013; Zhang et al., 2014a). Besides the spherical MMPs (sMMPs), we have identified
82 another morphotype, the ellipsoidal or pineapple-like MMPs (eMMPs) in the Mediterranean

Sea (Lefèvre et al., 2007; Chen et al., 2016), the China Sea, and the Pacific Ocean (Zhou et al., 2012; Chen et al., 2015; Du et al., 2015; Dong et al., 2016; Teng et al., 2018). Approximately 60 cells aggregate into four to six interlacing circles to form a ~ 5–10 μM ellipsoidal entity. Both morphotypes synthesize magnetite or greigite, or both, magnetosomes. The common features for the two morphotype MMPs are that the periphery surface of their cells is covered by thousands of flagella whilst the inner surface surrounds a core lumen. Both display two kinds of typical swimming behaviors of MMPs when inspected in droplets. North-seeking MMPs swim and accumulate at the north edge of droplets. Randomly, they escape from the north edge and swim southward with acceleration. At variable distances, MMPs decelerate, stop the motility, and swim with acceleration northward back to the north edge (Rodgers et al., 1990; Simmons et al., 2004; Zhou et al., 2012; Zhou et al., 2013; Zhang et al., 2014a; Chen et al., 2015; Chen et al., 2016). South-seeking MMPs exhibit a similar escape motion, but in the opposite direction (Lins de Barros et al., 1990; Lins et al., 1999; Keim et al., 2004a; Greenberg et al., 2005). This behavior is referred to as escape motility or ping-pong motion. In addition, illumination with blue, violet, or UV light triggers the MMPs to swim away from the droplet edges opposite to the magnetotaxis direction, which is referred to as a photophobic response or is sometimes miscalled negative phototaxis (Shapiro et al., 2011; Zhou et al., 2012; Zhou et al., 2013; Zhang et al., 2014a; Chen et al., 2015; Chen et al., 2016)

To gain more insight into the bacterial multicellularity, we performed multiple microscopy analyses of ellipsoidal MMPs. The results obtained contributed to better understanding about diversity, architecture, reproduction and motility of this peculiar multicellular prokaryote model organism.

Results

Diversity of multicellular magnetotactic prokaryotes

In general, single phylotype of MMPs was identified at a given sampling site (Abreu et al., 2007; Wenter et al., 2009; Zhou et al., 2012; Zhou et al., 2013; Kolinko et al., 2014; Zhang et al., 2014a; Chen et al., 2015; Chen et al., 2016). An exception has been reported by Simmons et al. (Simmons and Edwards, 2007), they found five phylotypes of spherical MMPs in samples collected from Little Sippewissette salt marsh (Falmouth, MA, USA). The low natural abundance and similar morphology of MMPs prevented analysis of their diversity. Recently, Li et al. (Li et al., 2017) applied a coordinated FISH-SEM analysis procedure to efficiently identify the phylotypes of magnetotactic bacteria with simultaneous characterization of their magnetic crystals. Here, we used this procedure to assess the diversity of ellipsoidal MMPs of the Mediterranean Sea (Fig. 1*A*). We collected magnetotactic bacteria (MTB) by racetrack magnetic enrichment and obtained five 16S rRNA gene sequences that potentially belonged to MMPs. One of them (SF-1) was identical to the previously identified ellipsoidal MMPs collected from this site (Chen et al., 2016), and

the others shared higher than 90% identity with SF-1. Using correlative FISH-SEM analysis, we confirmed the authenticity of the ellipsoidal MMPs SF-2 to SF-5 and showed species-dependent cell morphology and magnetosome arrangement in the MMPs (Fig. 1*B, C, D,* and *E*). These results unambiguously show the diversity of ellipsoidal MMPs at this sampling site. In parallel, we also used magnetic micromanipulation to sort MMPs collected from Lake Yuehu and Six-Fours-les-Plages (see Experimental Procedures), and amplified and sequenced their 16S rRNA genes as previously reported (Kolinko et al., 2014; Zhang et al., 2014a; Chen et al., 2015; Chen et al., 2016). In total, we obtained 11 new 16S rRNA gene sequences, identifying five species belonging to three genera of spherical MMPs and six species belonging to three genera of ellipsoidal MMPs (Fig. 2*A*), using a 97% and 95% sequence identity as the threshold for classifying species and genera, respectively (Tindall et al., 2010). Our study has therefore extended the total number of identified spherical and ellipsoidal MMPs to eleven species belonging to six genera and nine species belonging to six genera, respectively. They formed branches of a MMP clade that were affiliated with *Deltaproteobacteria* but were distinguished from the multicellular myxobacteria (Fig. 2*B*). The worldwide distribution and the great diversity of species justify the consideration of MMPs as a distinct taxonomic group of multicellular prokaryotes.

Cellular arrangement within ellipsoidal MMPs

Previously we have reported the architecture of ellipsoidal MMPs using fluorescence microscopy, transmission electron microscope (TEM), scan electron microscope (SEM), and focused ion beam SEM (FIB-SEM) (Zhou et al., 2012; Chen et al., 2015; Chen et al., 2016; Leao et al., 2017). Approximately 40–80 cells arrange in interlacing circles with a pineapple-like ellipsoidal morphology. Partly because of the MMP size, the resolution that can be achieved by these microscopy techniques is limited. In addition, knowledge about overall three-dimensional arrangement of cells in ellipsoidal MMPs needs to be improved. HPF/FS fixation is an optimal method to preserve the structures present in the living cell up to a thickness of 200 µm. Here, we used HPF/FS, for the first time, in combination with TEM and fluorescence confocal microscopy to study the ultrastructure of MMPs. As previously reported (Leao et al., 2017) but with more detail, we observed the conspicuous periphery-core architecture (Fig. 3*A, B, C, E* and *G*), an axisymmetrical arrangement of cells along the eMMP longitudinal axis (Fig. 3*A*), a "open space" at one end (Fig. 3*A*, top) and a core lumen in the center of ellipsoidal MMPs (Fig. 3*G* and *K*). We also found at surface of the MMPs, flagella (Fig. 3*A* and *I*), and, in the cytoplasm, magnetite magnetosomes (Fig. 3*A, B, D, F, G* and *H*), lipid granules, (Fig. 3*A, D, G* and *I*), and periphery bars at the external side of the cells (green arrows in Fig. 3*J* and *SI,* Fig. S2).

Besides these structures, ultrathin sections of HPF/FS samples unveiled an unreported electron dense dashed line surrounded the outermost surface (Fig. 3*A*, *G*, *H*, and *J*, yellow arrows). The dashes were approximately 11.6 x 20.7 nm (average of 193 points from two MMPs) and aligned with an interval distance of 10.3 nm (average of 183 points from two MMPs) along the perimeter of a matrix outside the outer membrane of the MMPs (Fig. 3*G*, *H*, and *J*). The dashed lines on two successive ultrathin sections arranged in a similar pattern (*SI*, Fig. S1). Therefore, it is likely that the regular distributed dashes are a cut-view of a lattice that holds the cells together (Fig. 3*G*, *H*, and *J*). Underneath the matrix layer, there are the well-preserved three-layer structures of the outer membrane, peptidoglycan, and the inner membrane (Fig. 3*G*, *H*, *I* and J). The high quality of preservation unveiled unambiguously that juxtaposed membranes tightly connect cells together to assemble into a multicellular entity (Fig. 3*D* and *G*, red asterisks). Close to the periphery side of the inner membranes, a fence-like structure (f) was observed in some cells (cell 4 in Fig. 3*G* and *J*), which recalls the structure of photosynthetic membrane lamellae in prokaryotic cells. The laser confocal analysis and reconstitution of ultrathin section images clearly revealed that ellipsoidal MMPs consist of only one layer of cells that are all connected to the core lumen (Fig. 3*C*, *E*, *SI* Movie 1). Taken together, juxtaposed membranes adhere cells together surrounding the core lumen to achieve a one-layer hollow structure that is held by a well-patterned lattice at the surface of ellipsoidal MMPs.

Reproduction of ellipsoidal MMPs

Ellipsoidal MMPs consist of cells that are arranged axisymmetrically along the long body axis and radially on the short axis dissection. We investigated how they reproduce to maintain the inherent periphery–core architecture and a magnetic polarity. Ultrathin sections of HPF/FS- or chemically fixed MMPs revealed that all dividing cells exhibit a unilateral indentation of the cell wall from the periphery towards the core lumen (Fig. 4*B* and *C*, red asterisks and yellow triangles). The high-quality preservation of the membrane structures by HPF/FS exposes the process of constituent cell division. As shown on two successive ultrathin slices of an HPF/FS-fixed eMMP (Fig. 4*D* and *E1*), outer membranes bend inward from the peripheral surface and the two sides then join together, doubling the thickness, and invaginate into the cytoplasm. The constriction furrow penetrates unilaterally into the cytoplasm without initiating indentation of the membranes at the core lumen side, even when the constriction furrows into three-fifths of the depth of the cytoplasm (Fig. 4*D*, *E1*, *E2*, and *E3*). We analyzed ultrathin sections with the core lumen of eleven MMPs and found approximately 50% of cells having a constriction furrow. In all cases, we observed the indentation occurring unilaterally only from the periphery toward the lumen. The inward bending and doubling thickness of the outer membrane at the onset of cytokinesis displayed the same structure as the outer membrane between two neighboring cells (Fig. 4*D* and *E* compared to *F*, red asterisks). As shown in Fig. 4*D*, the outer membranes connect the cells

194 together. Therefore, the juxtaposed membrane implies a characteristic adhesion of MMP
195 cells. Moreover, the surface lattice and matrix seem to prevent the cells from separation from
196 the aggregates after the division. These observations strongly suggest the evolution of MMP
197 toward multicellularity via the mechanism of incomplete separation of offspring (Bonner,
198 1999).
199 Further fluorescence confocal microscopy inspection of cells shows membranes that
200 separated neighboring cells on the surface stack images (Fig. 4*G1*, yellow arrows). However,
201 on the deeper stack images in some cases, the membranes disappeared progressively first at
202 the center, leading to 'H-shaped' cells (Fig. 4*G2* to *G4*), and then at the opposite corners of
203 the dividing cells (*SI* Movie S2). These results are consistent with the hypothesis that
204 unilateral constriction of cell envelope occurs from the periphery toward the core lumen
205 parallel to the long axis of MMPs. Moreover, the "H-shaped" cells that were previously
206 observed using FIB-SEM microscopy reflect a stage of cell division instead of a permanent
207 morphology of MMP cells. Notably the HPF/FS slice in Fig. 4*H* shows the split of an
208 ellipsoidal multicellular magnetotactic prokaryote, which corresponds to one state of the
209 division process revealed by confocal microscopy (Fig. 5*I*). A collection of confocal analyses
210 corroborated the hypothetical unidirectional split of the eMMP entity using fluorescence
211 staining to visualize the membrane (Fig. 4*I*, *SI* Movie S3) or intracellular lipid granules (Fig.
212 4*J*, *SI* Movie S4).

Bounce motion, axial magnetotaxis, and magnetotactic-photokinesis of ellipsoidal MMPs

Multicellular magnetotactic prokaryotes possessed multiple magnetosome chains arranged along their long axis (Fig. 5*A*) and were covered by flagella (Fig. 5*B*). The HPF/FS thin section images showed that the flagella have a diameter of approximately 22 nm with an interval distance of 68 nm (Fig. 3*I*). If the flagella are separated by equal longitudinal and latitudinal distances, we can assume a flagella density of 1 flagellum per 8100 nm squares (123 flagella per µm square), which could lead to approximately ten thousand flagella on a 4 x 8 µm MMP. It is similar to the 147 flagella motors per µm square estimated for spherical MMPs (Silva et al., 2007). The multiple bundles of magnetosomes and thousands of flagella underpin the canonical magnetotactic behavior of MMPs. Previous studies of MMPs swimming in droplets have shown the typical escape and photophobic motilities. To gain deeper insight into these behaviors we further analyzed MMPs swimming in microfluidic channels (see Experimental Procedures) to mitigate the air-liquid-solid border effect, and irregular light transmission that occurs in droplets.

The swim velocity of ellipsoidal MMPs collected from environmental samples when compared one to another, displayed up to a ten-fold variation and the velocities decreased progressively as the observation time increased. We observed eMMP swimming northward with an average velocity of 34.2 ± 14.7 µm/s (n=12). When they performed escape or ping-pong motion eMMPs swam southward at 20.0 ± 9.3 µm/s (n=14) with instantaneous

232 acceleration ranging from 87.6 to 6.3 μm/s^2, which was followed by a return northward
233 swimming at of 13.5 ± 6.1 μm/s (n=10). Despite the substantial variation of velocity among
234 individuals the pattern of each type of swimming behavior was very well conserved and
235 examination of instantaneous velocity change of a given multicellular magnetotactic
236 prokaryote in response to an environmental stimulus is meaningful. We observed backward
237 motility of eMMPs accumulated at north side in microchannels (Fig. 5*C*, *SI* Movie 5).
238 Notably the backward motion in microchannels shares a similar pattern with the escape or
239 ping-pong motion of MMPs in droplets; eMMP swim to and accumulate at the north edge in
240 droplets or in microchannels, where some of them randomly make a backward swim with
241 acceleration. The mechanism involved in eMMPs sensing of microchannel walls might be
242 different from that of sensing the surface/border of the droplets although both the wall and
243 the border prevent MMPs from further northward swim. We also observed a conspicuous
244 backward motion when MMPs encountered obstacles (Fig. 5*D*, *SI* Movie 6). The channel
245 walls and obstacles blocked the forward north-seeking motility and triggered the MMPs to
246 swim backwards in order to circumvent the obstacles. Hence, we propose that the two
247 behaviors are considered a bounce motion. Moreover, at times MMPs randomly changed
248 their swimming direction southward and subsequently changed back to a north-seeking swim
249 (Fig. 5*E*, *SI* Movie 7), which is typical behavior of axial magnetotaxis (Bazylinski and
250 Frankel, 2004). The stochastic backward motion may play a similar physiological function to

the tumbling of *Escherichia coli* that allows bacteria to randomly explore the favorable direction in which to go. It is noteworthy that the backward swims in bounce motion and axial magnetotaxis started with the highest acceleration (red arrows and 'ac' in Fig. 5*D* and 5*E*) and had higher instantaneous velocity than the forward swim (red curves versus blue curves).

To characterize the photosensitive magnetotaxis of MMPs in microchannels, we applied two light-sources, i.e. a transmission light for observation and imaging and a UV (385 nm, 203 $\mu W/cm^2$) epi-illumination on a defined area for analyzing the photo-effect on swimming behavior. The swimming of MMPs was maintained within the illumination spots via application of an alternate uniform magnetic field (10 Gs, 0.5 Hz) in order to periodically reverse the swimming direction of MMPs before they left the illumination area. As shown in Fig. 5*F1*, an eMMP initially swam northward at 100 μm/s in the UV spot (green track). After the reversal of the field direction, the MMP immediately reversed its swimming direction to keep the north-seeking swim (Fig. 5*F1* the U-turn of the green dot track, 3*F2* the gap of green track at frame 40 and the change of velocity from positive to negative). Approximately 0.2 seconds later, the MMP suddenly changed its swimming direction to southward (red arrow and "r") with an acceleration (ac) that doubled the velocity, reaching approximately 200 μm/s (Fig. 5*F1*, *SI* Movie 8 and Movie 9). Therefore, the illumination resulted in not only the

269 photophobic response (*SI* Movie 10), but also in photokinesis of the magnetotaxis, i.e. a
270 change to the direction and velocity of motility.

271 **Discussion**

272 Our structure and behavior analyses unveil hallmark features of multicellularity that
273 distinguishes MMPs from other extensively studied multicellular bacteria. Both myxobacteria
274 and MMPs are affiliated with *Deltaproteobacteria* (Fig. 2*B*). Lying on the boundary between
275 uni- and multicellular organisms, myxobacteria grow and divide as proper unicellular Gram-
276 negative bacteria. However, they feed socially via collective predation. Moreover, under
277 starvation conditions, hundreds of thousands of cells form compact and symmetric structures,
278 i.e. fruiting bodies that confer on myxobacteria selective advantages for spore dispersion and
279 cooperative-feeding (Kaiser, 2001). On the contrary, MMPs are patterned, permanent
280 multicellular entities. They are constructed via tight cell membrane juxtaposition and an outer
281 matrix envelope. The spherical and ellipsoidal morphotypes of MMPs display different
282 assembly symmetries. The structures of the well-studied spherical MMPs consist of 15–40
283 cells that are arranged with a helical symmetry into a mulberry-like morphology (Farina et
284 al., 1983; Bazylinski et al., 1990; Farina et al., 1990; Lins de Barros et al., 1990; Mann et al.,
285 1990; Rodgers et al., 1990; Lins et al., 1999; Keim et al., 2004b). Although the short-axis
286 dissection of ellipsoidal MMPs exhibits radial symmetry like spherical MMPs, but only the
287 ellipsoidal MMP cells axisymmetrically assemble into several rows to form a pineapple-like

morphology. At present no unicellular stage has been observed for MMPs ((Keim et al., 2004a; Keim et al., 2004b; Abreu et al., 2006; Zhou et al., 2012; Abreu et al., 2013; Zhang et al., 2014a; Chen et al., 2015; Chen et al., 2016), and FISH in this study). Our phylogenetic analysis, based on 16S rRNA gene sequences, revealed that the MMP cluster is located distantly to myxobacteria and other unicellular magnetotactic bacteria (Fig. 2*B*). Interestingly, the genes involved in magnetosome biosynthesis are well conserved among uni- and multicellular magnetotactic bacteria from the *Deltaproteobacteria* class (Leao et al., 2017). This result cannot distinguish between acquisitions by nonmagnetic multicellular microbes of magnetosome coding genes via horizontal gene transfer from evolution of MMPs from unicellular magnetotactic *Deltaproteobacteria*. Future genomic phylogenetic analyses should shed light on the evolution mechanism of MMPs. The data presented here support the hypothesis that myxobacteria and MMPs gained their multicellularity in separate events.

Coordinated swimming behavior is a fundamental feature that emerged during the evolution of multicellularity. The paradigm of bacterial chemotaxis is underpinned by intracellular diffusion of phosphorylated proteins and their binding to flagellar motors to steer the swimming behavior in response to environmental stimuli (Wadhams and Armitage, 2004). MMPs exhibit a highly complex motion. In addition to the escape swim and photophobic response, here we showed the bounce motion, axial magnetotaxis, and magneto-photokinesis behavior of ellipsoidal MMPs. While unicellular magnetotactic bacteria display aero-

307 magnetotaxis and photophobic behavior (Frankel et al., 1997; Zhu et al., 2010), magneto-
308 photokinesis has been observed only for multicellular magnetotactic prokaryotes. MMPs
309 dwell in intertidal sediments as deep as 30 cm and undergo seasonal, and probably also daily,
310 vertical movement in response to nutrient distribution changes (Liu et al., 2018). Shapiro et
311 al. have suggested that photophobic behavior enables MMPs to optimize their location to
312 adapt to circadian variation of chemical gradients and light intensity (Shapiro et al., 2011).
313 Indeed genes involved in controlling circadian rhythm were found in the genomes of
314 spherical (Abreu et al., 2013) and ellipsoidal MMP strain SF-1 (*SI* Table S1). The bounce
315 motility and photokinesis capacity may be selective strategies for MMPs to move to
316 favorable places in sediments. Moreover, MMPs swim faster than most unicellular bacteria
317 and have large sizes, which imply an advantage in mitigating predation risk.
318 Bacterial photo-sensing might rely directly on dedicated photoreceptor systems or indirectly
319 on the products of photosynthesis or other illumination by-products, i.e. reactive oxygen
320 species, ATP, change of intracellular redox or force proton motif. The fence-like structure
321 (Fig. *3J*), which looks like photosynthetic membrane lamellae, could be an appropriate
322 candidate for accommodating photoreceptors involved in MMPs photo-sensing. Multicellular
323 magnetotactic prokaryotes displayed a helical trajectory of swimming and were illuminated
324 with UV-light perpendicularly to the translation direction. They changed the magnetotaxis
325 direction and velocity suddenly within the illumination area. Therefore, the magneto-

photokinesis is unlikely to be a result of the detection of an intracellular spatial light gradient. The sudden change of swim direction under constant illumination would suggest a cumulating effect of periodical exposure of photoreceptive structures to UV-light or production of harmful by-products. Therefore, multicellular magnetotactic prokaryotes reversed their swimming direction to escape from the deleterious light. It remains an enigma how thousands of flagella of 60–80 cells coordinate their rotations to propel the helical translation of MMPs. Therefore, the mechanism that governs the change of magnetotaxis direction is inexplicable. Both HPF/FS section and confocal data revealed that the core lumen connects all cells in a MMP, and the lumen thus might play a crucial role in the communication required to regulate the operation of flagella at the surface.

Reproduction of MMPs shows some particularities compared to other multicellular prokaryotes. Until now, no single-cell stage has been observed in the life cycle of MMPs (Keim et al., 2004a; Keim et al., 2004b; Abreu et al., 2006; Abreu et al., 2007; Abreu et al., 2013). Keim et al. have proposed that spherical MMPs reproduce by two major steps: division of individual cells via invaginations of the cell membrane at the external side, and "8"-shaped torsion fission of MMPs into two equal spheres (Keim et al., 2004b). Here, the highly preserved structure of ultrathin sections unambiguously reveals the unilateral constriction of MMP cells (Fig. 4). It has been reported recently that nematode symbiont rod-shaped *Gammaproteobacteria* initiate division by membrane invagination only at the

345 proximal pole that is attached to the host cuticle (Pende et al., 2018). The fission progresses
346 by membrane invagination at the distal end and the two constriction furrows penetrate
347 longitudinally towards the center until there is a complete division. Similarly, electron cryo-
348 tomography analysis of unicellular bacteria reveals that some dividing cells from eight
349 bacterial species initiate indentations of the cell envelope on only one side of the cells at the
350 early-constriction state (Yao et al., 2017). Subsequently, all mid-constriction cells exhibit
351 constriction on both sides of the cell body, and the division furrows converge into a neck-like
352 structure in the late-constriction cells, which indicates bidirectional division of these cells.
353 Cyanelles are primitive photosynthetic organelles of protists *Cyanophora paradoxa*. During
354 their reproduction a shallow furrow starts asymmetrically on one side of the division plane,
355 resulting in kidney-shaped cyanelles. Subsequently the furrow extends, covers, and deepens
356 around the entire circumference of the division plane, leading to dumbbell-shaped cyanelles
357 and a complete division (Chang et al., 2009). The MMP cells are distinguished from other
358 asymmetrically constricted unicellular cells by the apparent absence of bilateral indentations
359 of the membrane even at late stages of the division. The periphery–core architecture of
360 MMPs might prevent the symmetric bilateral constriction. The periphery bars, which are
361 located underneath the outer curved membrane and close to the magnetosome chains in MMP
362 cells (Fig. 3*J*, *SI Appendix*, Fig. S2), might play a role in determining the onset of unilateral
363 cell constriction. Interestingly, the unicellular magnetotactic bacterium *Magnetospirillum*

gryphiswaldense reproduces via asymmetric, wedge-like constriction of the cell wall at the division site, which leads to snapping of the magnetosome chain into halves in the two offspring with minimal magnetostatic attraction (Katzmann et al., 2011). Unilateral indentation of the MMP cell wall seems to be a similar mechanism of the segregation of magnetosome chains in the multiple daughter cells that remain tightly connected after division.

The lack of MMP cultures prevents detailed study of the mechanisms of cell and entity divisions. Whole-genome sequencing and analysis might circumvent this obstacle. Moreover, it is crucial to develop a dedicated microscope device in order to determine precisely the wavelength spectra that trigger photokinesis and to perform real-time inspection of the MMP lifecycle in microchannels. Using multicellular magnetotactic prokaryotes as a novel model of multicellular organisms could provide a different way of thinking about the evolution of multicellularity. The periphery–core architecture restricts the mechanisms that govern cell division, cell-cell adhesion and communication, swimming coordination, and distinguishes MMPs from the filamentous cyanobacteria and actinomycetes.

Experimental Procedures

Phylogenetic analysis

Sediment samples were collected from Six-Fours-les-Plages (43°07’N, 5°79’E) of the Mediterranean Sea, or Lake Yuehu (37°21’N, 122°34’E) of the China Sea. Magnetotactic

bacteria were magnetically enriched using the race-track method (Wolfe et al., 1987). The 16S rRNA genes were directly amplified from the collected samples and sequenced, or after further collection of MMPs by magnetic manipulation microsorting, and then amplified and sequenced as previously reported (Chen et al., 2015). The ellipsoidal MMPs were sorted using a TransferMan ONM-2D micromanipulator and an IM-9B CellTram Oil manual hydraulic pressure-control system installed on an IX51 microscope equipped with a 40 × LD objective (all from Olympus). One droplet (20 μl) containing magnetically collected MMPs and several droplets of 20 μl filter-sterilized (0.2 μm pore size) sample water were placed onto a glass slide. The ellipsoidal MMPs were transferred using micromanipulator from magnetic collections successively to the droplets of filter-sterilized sample water. In the transferred washing steps, the MMPs were aspirated and expulsed by the glass capillary (at least 10 times) for removal of contaminants and extracellular DNA (Chen et al., 2015). Finally, two to ten purified MMPs were directly transferred to one reaction tube containing 3 μl of PBS, which was in REPLI-g Single Cell Kit (cat # 150343; QIAGEN, German). The PBS-suspended sample was frozen and thawed repeatedly, and the WGA reaction was carried out using the REPLI-g Single Cell Kit. Only the samples containing single homogenous 16S rRNA sequence were used in this study.

Characterization of swimming behavior

Swimming behaviors of MMPs were analyzed either in droplets with the optical microscopes Olympus BX51 or Nikon TiE (Chen et al., 2015), or in microfluidic channels with a Magnetodrome device (2D and 3D µ-Slide Chemotaxis channels, Ibidi, GmbH, Germany; or home-made channels as described in (Zhang et al., 2014b)). To characterize photokinesis behavior, we modified the Zeiss Axio Observer A1 microscope on the Magnetodrome device (Zhang et al., 2014b) by replacing the HBO 100 light source with Zeiss Colibri 7. A UV light (385 nm) at 203 µW/cm^2 was used to trigger photophobic and photokinesis behavior. The swimming of MMPs was maintained within the UV spot by application of an alternate uniform magnetic field (10 Gs, 0.5 Hz) in order to periodically reverse the swimming direction of MMP before they left the illumination area. The motility was analyzed using MTrackJ Plugins of ImageJ (Meijering et al., 2012).

Microscopy analyses

Routine optical microscopy observation was performed with Zeiss Axiostar Plus, Zeiss Axio Vert 200M, and Olympus BX51. To perform laser confocal analysis, MMPs were fixed with 1% paraformaldehyde for 1.5 hours at room temperature, stained with 15 µg/ml Nil red (for lipids), 7.5 µg/ml FM4-64 (for membranes), and 2µg/ml DAPI (for chromosomal DNA) and observed with the Olympus FV1000 microscope with laser 405 nm excitation and 425–475 nm emission for DAPI and 543 nm excitation and 555–655 nm emission for Nil Red and

FM4-64. Images were collected at a series of focal levels at 0.17 μm intervals. Three-dimensional image reconstitution was performed using ImageJ and Amira software.

Correlative FISH-SEM analyses were carried out on coverslips as described by Li et al. (Li et al., 2017). Briefly, we designed four probes that specifically target to the 16S rRNA gene sequences of ellipsoidal MMPs (*SI Appendix*, Table S2) and evaluated their specificity using the online probe evaluation tool Ribosomal Database Project (Cole et al., 2009; Cole et al., 2014). The MMP-specific probes were synthesized and fluorescently labeled with the hydrophilic sulfoindocyanine dye Cy3 at the 5' end. The universal bacterial probe EUB338 (Table S1) was fluorescently labeled with fluorescein phosphoramidite 200 FAM at the 5' end and used for FISH as a positive-control probe for bacteria (Amann et al., 1990). FISH observation was performed with a Nikon TiE microscope by following the protocols reported by Simmons and Edwards (Simmons and Edwards, 2007) and Li et al. (Li et al., 2017). The same coverslips were treated for SEM observation using a Zeiss Ultra-55 field-emission gun SEM (Carl Zeiss, Germany) operating at 5 kV (Li et al., 2017). General SEM morphology analyses of MMPs were carried out using a KVKV-2800B microscope as described by Chen et al. (Chen et al., 2015).

Transmission electron microscopy

Magnetotactic bacteria were pelleted, high-pressure frozen, freeze substituted, embedded in Epon resin (Medium Grade), as reported in (McDonald, 2014). Because only low amount of

MMPs could be collected from fresh environmental samples each time, cells of marine unicellular photobacterium cultures were added during HPF/FS preparation. Ultrathin sections (60–90 nm) were cut with an ultracryomicrotome (EM UC7 Leica) and stained with uranyl acetate and lead citrate (Reynolds, 1963). The samples were analyzed using a Tecnai 200KV electron microscope (FEI) and digital acquisitions were made using a numeric camera (Eagle, FEI). Alternatively, the grids were analyzed using STEM-HAADF for Z-contrast imaging, using a JEM-2100F microscope (JEOLLtd., Tokyo, Japan) operating at 200 kV equipped with a field emission gun, an ultra-high resolution pole piece and a Gatan energy filter (GIF2001) system (Gatan, Inc., Pleasanto, 242 CA, USA) to determine element composition. High resolution TEM images were analyzes with Fast Fourier Transform (FFT) procedure using ImageJ 1.52o software (http://imagej.nih.gov/ij/).

Acknowledgments

We thank A. Bernadac and Y. Pan for critical reading of the manuscript, A. Bernadac for suggestions for sample preparation and N. Petersen for Magnetodrome assistance. We are grateful to H. Zhang and F.X. Wang for their assistance in the coordinated FISH-SEM experiments. This work was supported by a funding from the Excellence Initiative of Aix-Marseille University - A*Midex, a French “Investissements d’Avenir” programme, by grants 41330962 and 41506147 from NSFC, grant 2018YFC0309904 from National Key R&D Program of China, grant XDB06010203 from the Strategic Priority Research Program and

457 grants from CNRS for LIA-MagMC. The FISH-SEM experiments were performed at the

458 IGGCAS, Beijing, China and were supported by a NSFC grant 41522402.

References

Abreu, F., Silva, K.T., Martins, J.L., and Lins, U. (2006) Cell viability in magnetotactic multicellular prokaryotes. *Int Microbiol* **9**: 267-272.

Abreu, F., Martins, J.L., Silveira, T.S., Keim, C.N., de Barros, H.G., Filho, F.J., and Lins, U. (2007) 'Candidatus Magnetoglobus multicellularis', a multicellular, magnetotactic prokaryote from a hypersaline environment. *Int J Syst Evol Microbiol* **57**: 1318-1322.

Abreu, F., Morillo, V., Nascimento, F.F., Werneck, C., Cantao, M.E., Ciapina, L.P. et al. (2013) Deciphering unusual uncultured magnetotactic multicellular prokaryotes through genomics. *ISME J* **8**: 1055-1068.

Amann, R.I., Krumholz, L., and Stahl, D.A. (1990) Fluorescent-oligonucleotide probing of whole cells for determinative, phylogenetic, and environmental studies in microbiology. *J Bacteriol* **172**: 762-770.

Bazylinski, D.A., and Frankel, R.B. (2004) Magnetosome formation in prokaryotes. *Nat Rev Microbiol* **2**: 217-230.

Bazylinski, D.A., Frankel, R.B., Garratt-Reed, A.J., and Mann, S. (eds) (1990) *Biomineralization of iron-sulfides in magnetotactic bacteria from sulfidic environments*. NY: Plenum Press New York.

Bonner, J.T. (1999) The origins of multicellularity. *Integr Biol* **1**: 27-36.

Chang, L.Y., Harduin-Lepers, A., Kitajima, K., Sato, C., Huang, C.J., Khoo, K.H., and Guerardel, Y. (2009) Developmental regulation of oligosialylation in zebrafish. *Glycoconj J* **26**: 247-261.

Chen, Y.R., Zhang, R., Du, H.J., Pan, H.M., Zhang, W.Y., Zhou, K. et al. (2015) A novel species of ellipsoidal multicellular magnetotactic prokaryotes from Lake Yuehu in China. *Environ Microbiol* **17**: 637-647.

Chen, Y.R., Zhang, W.Y., Zhou, K., Pan, H.M., Du, H.J., Xu, C. et al. (2016) Novel species and expanded distribution of ellipsoidal multicellular magnetotactic prokaryotes. *Environ Microbiol Rep* **8**: 218-226.

Claessen, D., Rozen, D.E., Kuipers, O.P., Sogaard-Andersen, L., and van Wezel, G.P. (2014) Bacterial solutions to multicellularity: a tale of biofilms, filaments and fruiting bodies. *Nat Rev Micro* **12**: 115-124.

Cole, J.R., Wang, Q., Fish, J.A., Chai, B., McGarrell, D.M., Sun, Y. et al. (2014) Ribosomal Database Project: data and tools for high throughput rRNA analysis. *Nucleic Acids Res* **42**: D633-642.

Cole, J.R., Wang, Q., Cardenas, E., Fish, J., Chai, B., Farris, R.J. et al. (2009) The Ribosomal Database Project: improved alignments and new tools for rRNA analysis. *Nucleic Acids Res* **37**: D141-145.

Dong, Y., Li, J., Zhang, W., Zhang, W., Zhao, Y., Xiao, T. et al. (2016) The detection of magnetotactic bacteria in deep sea sediments from the east Pacific Manganese Nodule Province. *Environ Microb Rep* **8**: 239-249.

Du, H.-J., Chen, Y.-R., Zhang, R., Pan, H.-M., Zhang, W.-Y., Zhou, K. et al. (2015) Temporal distributions and environmental adaptations of two types of multicellular magnetotactic prokaryote in the sediments of Lake Yuehu, China. *Environ Microb Rep* **7**: 538-546.

Farina, M., Esquivel, D.M.S., and Lins de Barros, H.G.P. (1990) Magnetic iron-sulphur crystals from a magnetotactic microorganism. *Nature* **343**: 256-258.

Farina, M., Lins de Barros, H., Motta de Esquivel, D., and Danon, J. (1983) Ultrastructure of a magnetotactic microorganism. *Biol Cell* **48**: 85-88.

Frankel, R.B., Bazylinski, D.A., Johnson, M.S., and Taylor, B.L. (1997) Magneto-aerotaxis in marine coccoid bacteria. *Biophys J* **73**: 994-1000.

Greenberg, M., Canter, K., Mahler, I., and Tornheim, A. (2005) Observation of magnetoreceptive behavior in a multicellular magnetotactic prokaryote in higher than geomagnetic fields. *Biophys J* **88**: 1496-1499.

Hore, P.J., and Mouritsen, H. (2016) The Radical-Pair Mechanism of Magnetoreception. *Annu Rev Biophys* **45**: 299-344.

Johnsen, S., and Lohmann, K.J. (2005) The physics and neurobiology of magnetoreception. *Nat Rev Neurosci* **6**: 703-712.

Kaiser, D. (2001) Building a multicellular organism. *Annu Rev Genet* **35**: 103-123.

Katzmann, E., Muller, F.D., Lang, C., Messerer, M., Winklhofer, M., Plitzko, J.M., and Schuler, D. (2011) Magnetosome chains are recruited to cellular division sites and split by asymmetric septation. *Mol Microbiol* **82**: 1316-1329.

Keim, C.N., Abreu, F., Lins, U., Lins de Barros, H., and Farina, M. (2004a) Cell organization and ultrastructure of a magnetotactic multicellular organism. *J Struct Biol* **145**: 254-262.

Keim, C.N., Martines, J.L., Lins de Barros, H., Lins, U., and Farina, M. (2006) Structure, behavior, ecology and diversity of multicellular magnetotactic prokaryotes. In *Magnetoreception and Magnetosomes in Bacteria*. Schüler, D. (ed). Berlin Heidelberg: Springer-Verlag, pp. 104-132.

Keim, C.N., Martins, J.L., Abreu, F., Rosado, A.S., de Barros, H.L., Borojevic, R. et al. (2004b) Multicellular life cycle of magnetotactic prokaryotes. *FEMS Microbiol Lett* **240**: 203-208.

Kirschvink, J.L., and Gould, J.L. (1981) Biogenic magnetite as a basis for magnetic field detection in animals. *Biosystems* **13**: 181-201.

Kirschvink, J.L., Walker, M.M., and Diebel, C.E. (2001) Magnetite-based magnetoreception. *Curr Opin Neurobiol* **11**: 462-467.

Kolinko, S., Richter, M., Glockner, F.O., Brachmann, A., and Schuler, D. (2014) Single-cell genomics reveals potential for magnetite and greigite biomineralization in an uncultivated multicellular magnetotactic prokaryote. *Environ Microbiol Rep* **6**: 524-531.

Leao, P., Chen, Y.R., Abreu, F., Wang, M., Zhang, W.J., Zhou, K. et al. (2017) Ultrastructure of ellipsoidal magnetotactic multicellular prokaryotes depicts their complex assemblage and cellular polarity in the context of magnetotaxis. *Environ Microbiol* **19**: 2151-2163.

Lefèvre, C., Bernadac, A., Pradel, N., Wu, L.-F., Yu-Zhang, K., Xiao, T. et al. (2007) Characterization of mediterranean magnetotactic bacteria. *J Oce Univ China* **6**: 5-9.

Li, J., Zhang, H., Menguy, N., Benzerara, K., Wang, F., Lin, X. et al. (2017) Single-cellresolution of uncultured magnetotactic bacteria via fluorescence-coupled electron microscopy. *Appl Environ Microbiol* **83**: pii: e00409-00417.

Liedvogel, M., and Mouritsen, H. (2010) Cryptochromes--a potential magnetoreceptor: what do we know and what do we want to know? *J R Soc Interface* **7 Suppl 2**: S147-162.

Lins de Barros, H.G., Esquivel, D.M., and Farina, M. (1990) Magnetotaxis. *Sci Prog* **74**: 347-359.

Lins, U., Kachar, B., and Farina, M. (1999) Imaging faces of shadowed magnetite (Fe(3)O(4)) crystals from magnetotactic bacteria with energy-filtering transmission electron microscopy. *Microsc Res Tech* **46**: 319-324.

Liu, J., Zhang, W., Du, H., Leng, X., Li, J.-H., Pan, H. et al. (2018) Seasonal changes in the vertical distribution of two types of multicellular magnetotactic prokaryotes in the sediment of Lake Yuehu, China. *Environ Microb Rep* **10**: 475-484.

Mann, S., Sparks, N.H., and Board, R.G. (1990) Magnetotactic bacteria: microbiology, biomineralization, palaeomagnetism and biotechnology. *Adv Microb Physiol* **31**: 125-181.

McDonald, K.L. (2014) Rapid embedding methods into epoxy and LR White resins for morphological and immunological analysis of cryofixed biological specimens. *Microsc Microanal* **20**: 152-163.

Meijering, E., Dzyubachyk, O., and Smal, I. (2012) Methods for cell and particle tracking. *Methods Enzymol* **504**: 183-200.

Niessner, C., Denzau, S., Peichl, L., Wiltschko, W., and Wiltschko, R. (2014) Magnetoreception in birds: I. Immunohistochemical studies concerning the cryptochrome cycle. *J Exp Biol* **217**: 4221-4224.

Pende, N., Wang, J., Weber, P.M., Verheul, J., Kuru, E., Rittmann, S.K.R. et al. (2018) Host-polarized cell growth in animal symbionts. *Curr Biol* **28**: 1039-1051 e1035.

Reynolds, E.S. (1963) The use of lead citrate at high pH as an electron-opaque stain in electron microscopy. *J Cell Biol* **17**: 208-212.

Ritz, T., Adem, S., and Schulten, K. (2000) A model for photoreceptor-based magnetoreception in birds. *Biophys J* **78**: 707-718.

Ritz, T., Thalau, P., Phillips, J.B., Wiltschko, R., and Wiltschko, W. (2004) Resonance effects indicate a radical-pair mechanism for avian magnetic compass. *Nature* **429**: 177-180.

Ritz, T., Wiltschko, R., Hore, P.J., Rodgers, C.T., Stapput, K., Thalau, P. et al. (2009) Magnetic compass of birds is based on a molecule with optimal directional sensitivity. *Biophys J* **96**: 3451-3457.

Rodgers, F.G., Blakemore, R.P., Blakemore, N.A., Frankel, R.B., Bazylinski, D.A., Maratea, D., and Rodgers, C. (1990) Intercellular structure in a many-celled magnetotactic prokaryote. *Arch Microbiol* **154**: 18-22.

Schulten, K., Swenberg, C., and Weller, A. (1978) A biomagnetic sensory mechanism based on magnetic field modulated coherent electron spin motion. *Z Phys Chem NF* **111**: 1-5.

Shapiro, O.H., Hatzenpichler, R., Buckley, D.H., Zinder, S.H., and Orphan, V.J. (2011) Multicellular photo-magnetotactic bacteria. *Environ Microbiol Rep* **3**: 233-238.

Silva, K.T., Abreu, F., Almeida, F.P., Keim, C.N., Farina, M., and Lins, U. (2007) Flagellar apparatus of south-seeking many-celled magnetotactic prokaryotes. *Microsc Res Tech* **70**: 10-17.

Simmons, S.L., and Edwards, K.J. (2007) Unexpected diversity in populations of the many-celled magnetotactic prokaryote. *Environ Microbiol* **9**: 206-215.

Simmons, S.L., Sievert, S.M., Frankel, R.B., Bazylinski, D.A., and Edwards, K.J. (2004) Spatiotemporal distribution of marine magnetotactic bacteria in a seasonally stratified coastal salt pond. *Appl Environ Microbiol* **70**: 6230-6239.

Teng, Z., Zhang, Y., Zhang, W., Pan, H., Xu, J., Huang, H. et al. (2018) Diversity and Characterization of Multicellular Magnetotactic Prokaryotes From Coral Reef Habitats of the Paracel Islands, South China Sea. *Frontiers in Microbiology* **9**.

Tindall, B.J., Rossello-Mora, R., Busse, H.J., Ludwig, W., and Kampfer, P. (2010) Notes on the characterization of prokaryote strains for taxonomic purposes. *Int J Syst Evol Microbiol* **60**: 249-266.

Treiber, C.D., Salzer, M.C., Riegler, J., Edelman, N., Sugar, C., Breuss, M. et al. (2012) Clusters of iron-rich cells in the upper beak of pigeons are macrophages not magnetosensitive neurons. *Nature* **484**: 367-370.

Wadhams, G.H., and Armitage, J.P. (2004) Making sense of it all: Bacterial chemotaxis. *Nat Rev Mol Cell Biol* **5**: 1024-1037.

Wenter, R., Wanner, G., Schüler, D., and Overmann, J. (2009) Ultrastructure, tactic behaviour and potential for sulfate reduction of a novel multicellular magnetotactic prokaryote from North Sea sediments. *Environ Microbiol* **11**: 1493-1505.

Wiltschko, R., Gehring, D., Denzau, S., Niessner, C., and Wiltschko, W. (2014) Magnetoreception in birds: II. Behavioural experiments concerning the cryptochrome cycle. *J Exp Biol* **217**: 4225-4228.

Winklhofer, M., Abracado, L.G., Davila, A.F., Keim, C.N., and Lins de Barros, H.G. (2007) Magnetic optimization in a multicellular magnetotactic organism. *Biophys J* **92**: 661-670.

Wolfe, R., Thauer, R., and Pfennig, N. (1987) A "capillary racetrack" method for isolation of magnetotactic bacteria. *FEMS Microbiol Ecol* **45**: 31-35.

Yao, Q., Jewett, A.I., Chang, Y.W., Oikonomou, C.M., Beeby, M., Iancu, C.V. et al. (2017) Short FtsZ filaments can drive asymmetric cell envelope constriction at the onset of bacterial cytokinesis. *EMBO J* **36**: 1577-1589.

Zhang, R., Chen, Y.R., Du, H.J., Zhang, W.Y., Pan, H.M., Xiao, T., and Wu, L.F. (2014a) Characterization and phylogenetic identification of a species of spherical multicellular magnetotactic prokaryotes that produces both magnetite and greigite crystals. *Res Microbiol* **65**: 481-489.

Zhang, S.D., Petersen, N., Zhang, W.J., Cargou, S., Ruan, J., Murat, D. et al. (2014b) Swimming behaviour and magnetotaxis function of the marine bacterium strain MO-1. *Environ Microbiol Rep* **6**: 14-20.

Zhou, K., Zhang, W.Y., Pan, H.M., Li, J.H., Yue, H.D., Xiao, T., and Wu, L.F. (2013) Adaptation of spherical multicellular magnetotactic prokaryotes to the geochemically variable habitat of an intertidal zone. *Environ Microbiol* **15**: 1595-1605.

Zhou, K., Zhang, W.Y., Yu-Zhang, K., Pan, H.M., Zhang, S.D., Zhang, W.J. et al. (2012) A novel genus of multicellular magnetotactic prokaryotes from the Yellow Sea. *Environ Microbiol* **14**: 405-413.

Zhu, K., Pan, H., Li, J., Yu-Zhang, K., Zhang, S.-D., Zhang, W.-Y. et al. (2010) Isolation and characterization of a marine magnetotactic spirillum axenic culture QH-2 from an intertidal zone of the China Sea. *Res Microbiol* **161**: 276-283.

632 Figure legends

633 Figure 1. Identification of Mediterranean MMPs by correlative microscopy.

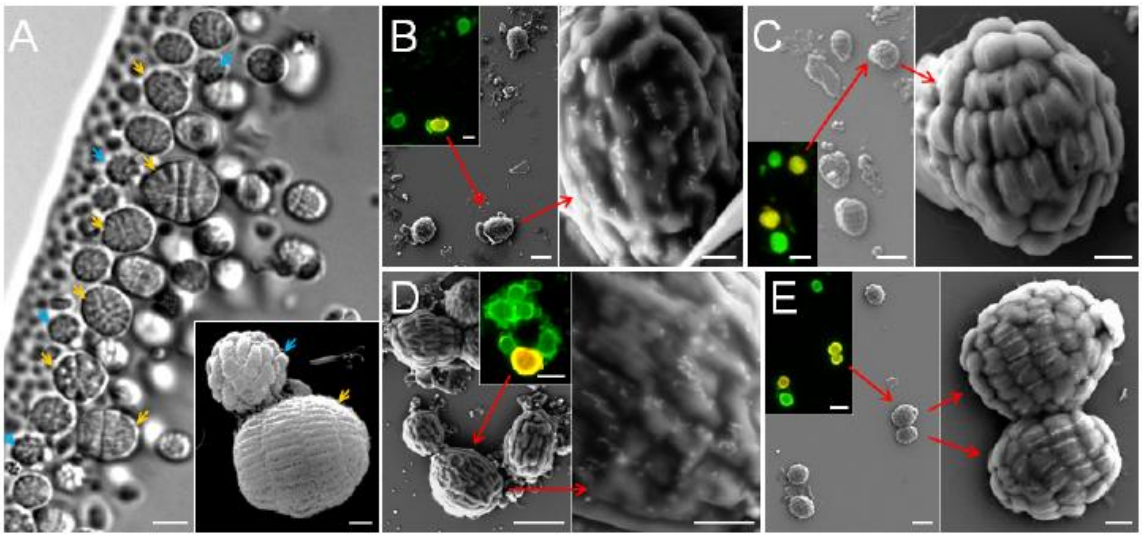

634

635 (A) Differential interference contrast (DIC) and scanning electron microscopy (inset)
636 micrographs of magnetically collected MTB accumulated at the north edge of a droplet
637 (Experimental Procedures). Blue and yellow arrows indicate spherical and ellipsoidal MMPs,
638 respectively. (B) to (E) Correlative FISH- (insets) SEM analysis of ellipsoidal MMPs. Green
639 color indicates bacteria hybridized only with the 5'-FAM-labeled universal bacterial probe
640 EUB338 and yellow color shows the MMPs hybridized with both the green universal probe
641 and the 5'-Cy3-labeled specific probes (SF-5, SF-3, SF-4, SF-2 in B, C, D, and E,
642 respectively). Red arrows correlate the MMPs on SEM micrographs with those specifically
643 hybridized in FISH insets. The images on the right panel of every set are the amplification of
644 the images from the left panel. Scale bars: 5μm in A, in FISH insets, and on left SEM panels
645 of B to E; 2 μm in inset of A; 1 μm on the right SEM panels of B to E.

Figure 2. Diversity and phylogenetic tree of MMPs.

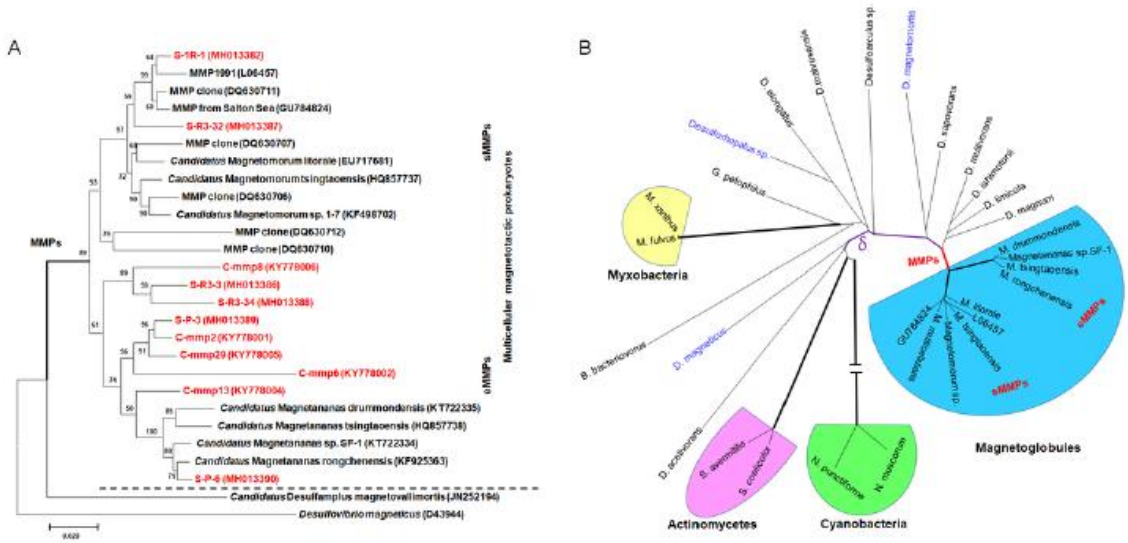

(A) Phylogenetic tree of currently identified MMPs. The species in red are newly identified in this study. The unicellular magnetotactic bacteria *Desulfamplus magnetomortis* and *Desulfovibrio magneticus* were used as outgroup references. The trees were constructed based on neighbor-joining analysis. Bootstrap values at the nodes are percentages of 1,000 replicates. The scale bar indicates 2% sequence divergence. The GenBank accession numbers of the sequences are given in parentheses. (B) Phylogenetic tree shows the approximate evolutionary position of MMPs with respect to myxobacteria (highlighted in yellow), actinomycetes (in pink), and cyanobacteria (in green). The branch length of cyanobacteria is truncated. All orders of *Deltaproteobacteria* are presented, including the unicellular magnetotactic bacteria (in blue) and the previously published MMPs.

Figure 3. Ultrastructure of ellipsoidal MMPs.

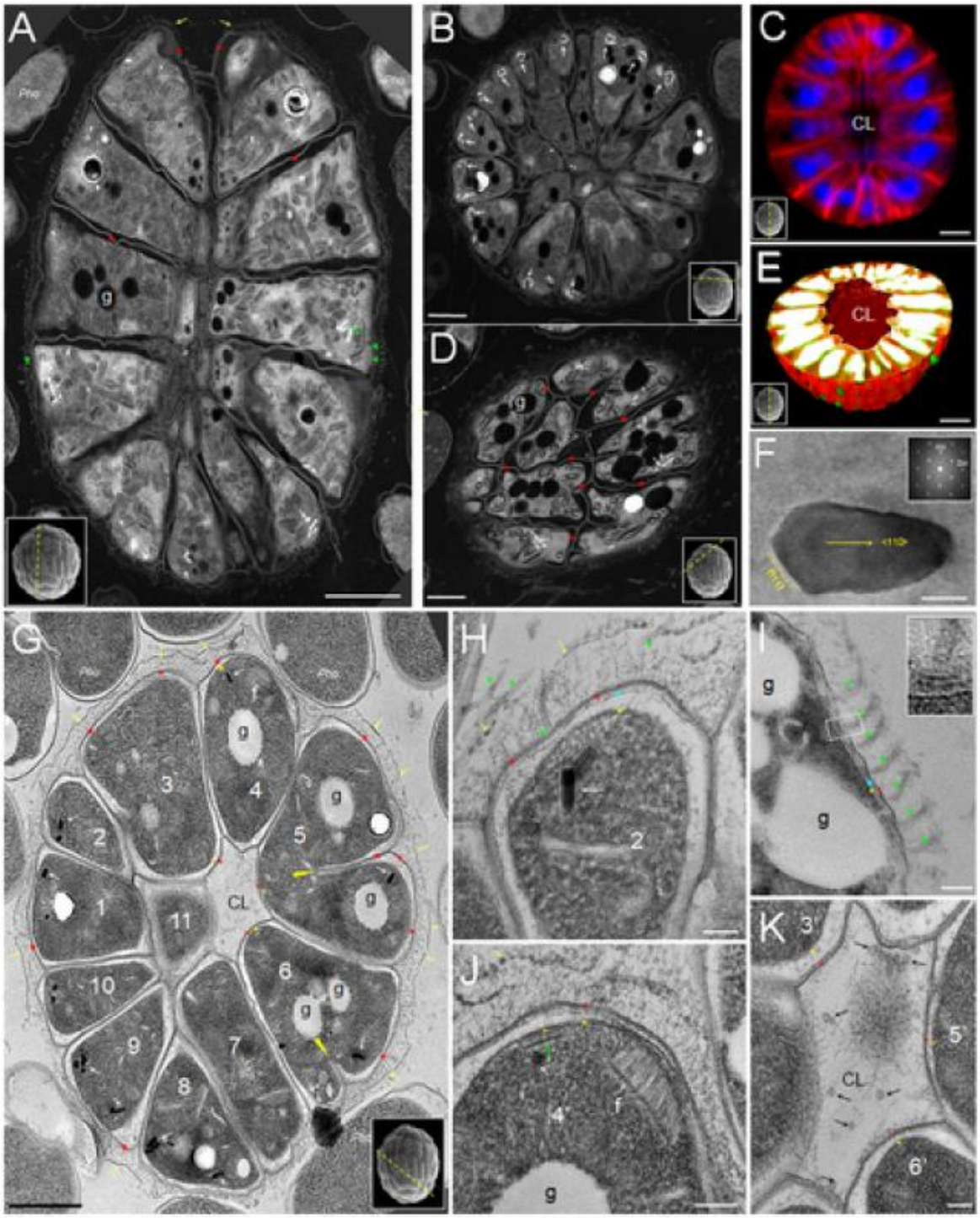

STEM-HAADF (Scan-TEM high-angle annular dark-field) mode (A, B and D) and TEM-bright field (BF) mode (G to K) micrographs of ultrathin sections of HPF/FS-fixed ellipsoidal MMPs. (C) and (E) are, respectively, a center stack or reconstitution of laser confocal images

of ellipsoidal MMPs; the membrane is stained by FM4-64 (red) and DNA by DAPI (blue) in (C) or artificial colors in (E). (F) shows a high-resolution image of a representative bullet-shaped magnetosome of ellipsoidal MMPs. From the corresponding fast Fourier transform (inset), it can de deduced that the magnetite elongation direction is <110> and that a prominent {111} basal plane is also visible. (G) shows cells surrounding a core lumen (CL). The yellow arrows visualize the dashed line on the surface of the MMP and the red and yellow asterisks indicate the outer and the inner membrane, respectively. White arrows point to the magnetosomes and the (f) is a fence-like structure. The yellow triangles indicate the extremity of the growing septa in cells 5 and 6. (H) is a magnified image of cell 2 showing the periphery structure that consists of flagella (green triangle), the dashed line, the outer and inner membranes, the peptidoglycan layer (blue asterisks), and magnetosomes. (I) shows flagella (green triangles) and a magnified image (inset) with likely the hook and basal body of a flagellum. (J) is a magnified image of cell 4 on a slice that is successive of the slice in (H). It visualizes the fence-like structure (f) and a periphery bar (green arrow). (K) is a magnified view of the core lumen (CL) on another successive slice of (G) with vesicles (black arrows) and filaments. The cell numbers correspond to the same numbers in panel (G). “g” are Nil red-stainable lipid granules. “pho” indicate the photobacterium cells (see Experimental Procedures). Scale bars: 1 µm in A, C, and G, 500 nm in B, D, and E, 100 nm

682 in H–K images. The insets in A to D and G illustrate the estimated cut direction of the

683 corresponding sections.

684 Figure 4. Division of constituent cells and reproduction of MMPs.

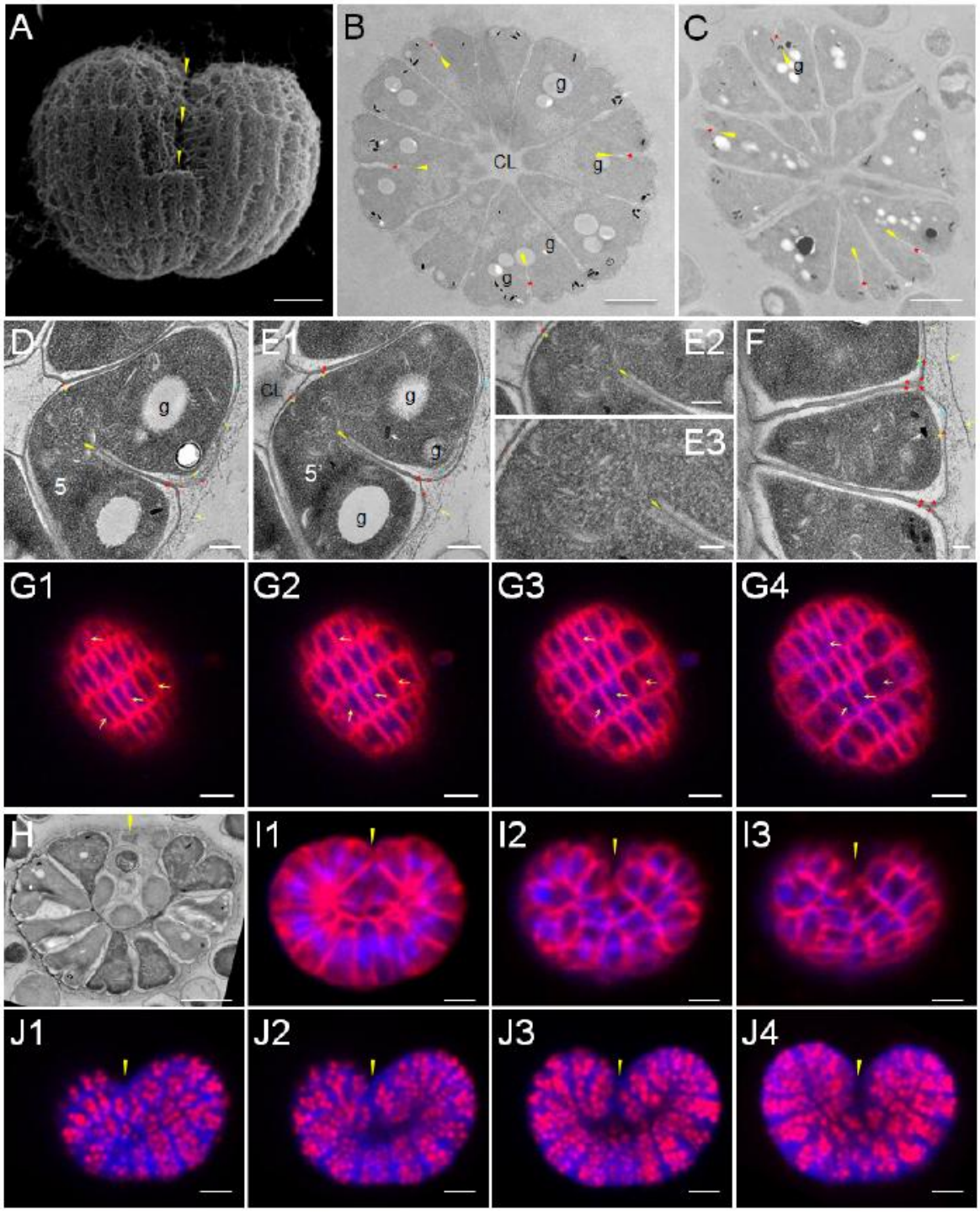

685

686 (A) is a SEM micrograph of a dividing MMP. Chemically (B) and HPF/FS- (C) fixed

ultrathin sections show the unilateral indentation of cell outer membranes (red asterisks and yellow triangles). (D) and (E) are two successive slices each of approximately 75 nm. The cell on the two slices is indicated with 5 and 5', that correspond to the same cell number 5 in Fig. 3G. (E2) and (E3) are magnified images of (E1) to show the end (yellow triangles) of the outer membrane (red asterisks) indentation. The yellow arrows (in D, E and F) visualize the dashed line on the surface of the MMP. The red, yellow and blue asterisks indicate the outer and inner membranes, and the peptidoglycan layer. White arrows point to the magnetosomes. (G), (I), and (J) are fluorescence confocal microscope images that show indentation of cell membranes of individual cells (yellow arrows in G) and division of a MMP (yellow triangles). (H) is a HPF/FS slice. DAPI staining (G, I, and J) was used to visualize chromosomes (blue spots), FM-4-64 (G and I, red) to visualize membranes and Nil red (J, red) to visualize lipids. Scale bars: 1 μm in A, B, C, G, H, I, and J and 100 nm in other images.

Figure 5. Bounce motion and photokinesis of ellipsoidal MMPs.

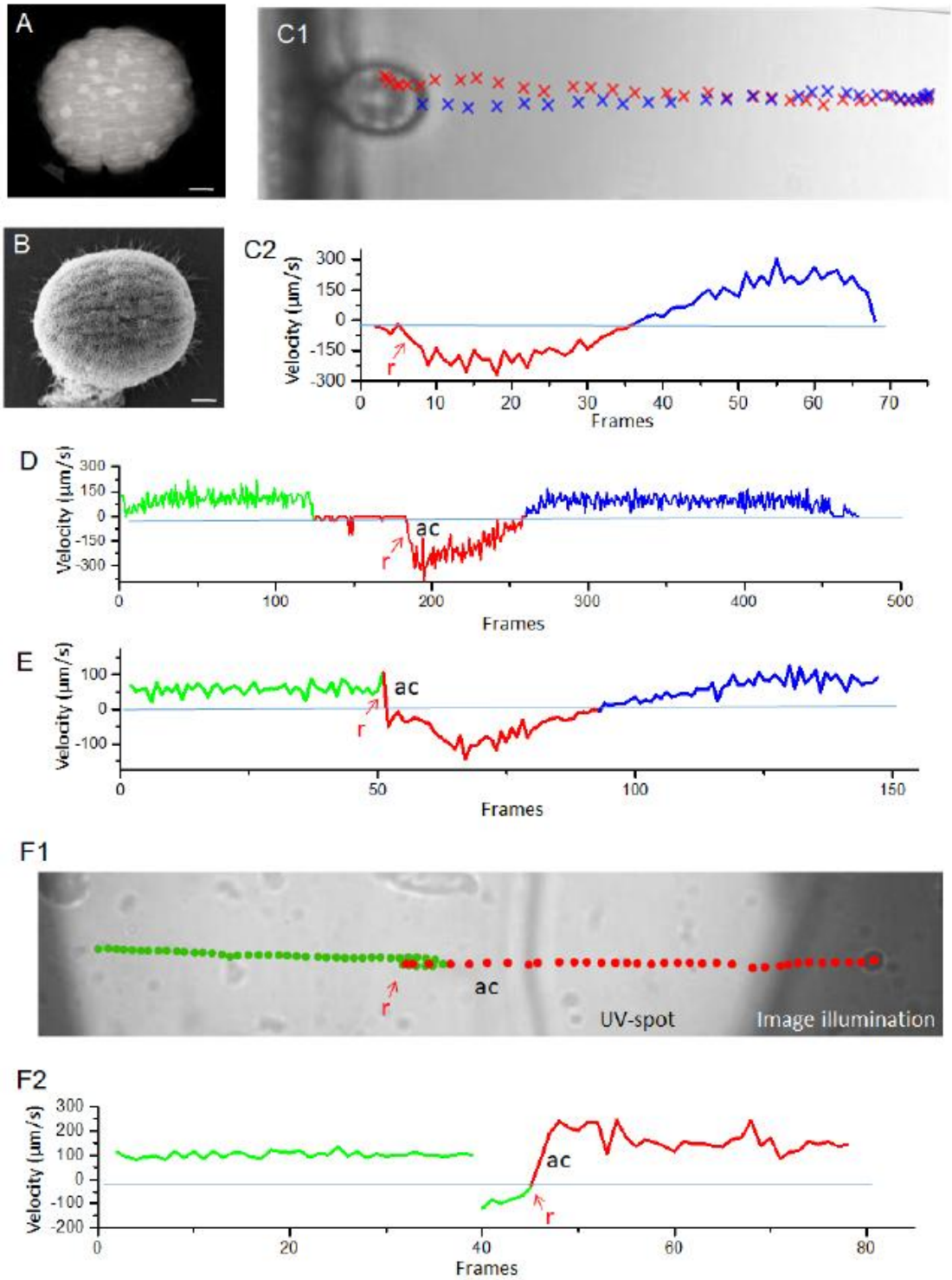

(A) Micrograph of scanning transmission electron microscope in high-angle annular dark-field mode (STEM-HAADF) shows the aligned magnetosome chains along the long axis of

the ellipsoidal MMP. (B) SEM micrograph reveals flagella on the surface of MMPs. (C) showcases the escape backward (red track) and return north-seeking forward (blue track) ping-pong swimming behavior (C1) and corresponding velocity (C2, positive is north-seeking). (D) and (E) show representative swimming behaviors when MMPs confronted obstacles or displayed axial magnetotaxis, respectively. Reversal of swimming direction to south-seeking is indicated by arrows “r” and red tracks. (F) shows a north-seeking MMP (green track) changing its swimming direction in response to the reversal of the alternate uniform magnetic field (10 Gs, 0.5 Hz). After 0.2 second it abruptly reversed its swimming direction to south-seeking (arrow “r” and red track) with acceleration (ac) and continued a south-seeking motion out of the UV spot. The movies were recorded at 60 frames per second (fps) for D and E and 30 fps for F.